

- (20) Bayer, E.; Nicholson, G. J.; Frank, H. *Amino Acid Analysis by Gas Chromatography*; Gehrke, C. W., Kuo, K. C. T., Zummel, R. W., Eds.; CRC Press: Boca Raton, FL, 1987; Vol. II, p 35-53.
- (21) Ernst, K. Ph. D. Thesis, University of Hamburg, 1984.
- (22) Saeed, T.; Sandra, P.; Verzele, M. J. *Chromatogr.* **1979**, *186*, 611-618.
- (23) Koppenhoefer, B.; Bayer, E. J. *Chromatogr. Libr.* **1985**, *32*, 1-42.

- (24) Feibush, B.; Cohen, M. J.; Karger, B. L. J. *Chromatogr.* **1983**, *282*, 3.

RECEIVED for review July 22, 1988. Accepted September 23, 1988.

# Scanning Electrochemical Microscopy. Introduction and Principles

Allen J. Bard,\* Fu-Ren F. Fan, Juhyoun Kwak, and Ovdia Lev

Department of Chemistry, The University of Texas, Austin, Texas 78712

**The technique of scanning electrochemical microscopy (SECM) is described. In this technique the electrolysis current that flows as an ultramicroelectrode tip (diameter ca. 10  $\mu\text{m}$ ) immersed in a solution is moved above a substrate surface is used to characterize processes and structural features of the substrate. Modes of operation considered include collection modes, where products electrogenerated at the substrate are detected at the tip (held at constant potential or operated in the cyclic voltammetric mode), and feedback modes, where the effect of substrate on the tip current is monitored. The feedback mode can be used with both conductive and insulating substrates and is less sensitive to electrical coupling between substrate and tip. An alternating current generation/collection mode is also described. Experimental results for the different modes of operation and proposed extensions of the SECM technique are presented.**

## INTRODUCTION

Scanning electrochemical microscopy (SECM) is a technique in which the current that flows through a very small electrode tip (generally an ultramicroelectrode with a tip diameter of 10  $\mu\text{m}$  or less) near a conductive, semiconductive, or insulating substrate immersed in solution is used to characterize processes and structural features at the substrate as the tip is moved near the surface. The tip can be moved normal to the surface (the  $z$  direction) to probe the diffusion layer, or the tip can be scanned at constant  $z$  across the surface (the  $x$  and  $y$  directions). The tip and substrate are part of an electrochemical cell that usually also contains other (e.g., auxiliary and reference) electrodes. The device for carrying out such studies involves means of moving the tip with a resolution down to the  $\text{\AA}$  region, for example, by means of piezoelectric elements or stepping motors driving differential springs, and is called a scanning electrochemical microscope. The abbreviation SECM is used interchangeably for both the technique or the instrument. The principle of an SECM operating in the generation/collection mode is illustrated in Figure 1B. As discussed below, other modes of operation are also used.

While the SECM resembles the scanning tunneling microscope (STM) (1) (Figure 1A) in its use of a tip to scan over a substrate surface and in the methods of moving the tip, there are fundamental differences in the principles of operation and range of applications. Since the STM depends upon the flow of a tunneling current between tip and substrate, the distance

between them is of the order of 1 nm or less and surface topographic  $x$ - $y$  resolution of only this size scale is usual (typical surface scan areas in STM are 30 nm by 30 nm). Moreover, even for STM studies in solution, the tunneling current is a nonfaradaic one (i.e., no chemical changes in solution components or substrate surface species occur because of the current flow), so that the tip current cannot be related directly to the substrate potential by consideration of the redox potentials of appropriate half-reactions. In SECM the current is carried by redox processes at tip and substrate and is controlled by electron transfer kinetics at the interfaces and mass transfer processes in solution, so that measurements at large spacings, e.g., the range of 1 nm to 10  $\mu\text{m}$ , can be made. This should allow probing of the diffuse and diffusion layers near the substrate through  $z$  scans of about 1 nm to 10  $\mu\text{m}$ , as well as lower resolution surface  $x$ - $y$  scans. In this case the tip current ( $i_T$ ) should be related to the potential of the tip ( $E_T$ ) and substrate ( $E_S$ ) by the usual electrochemical considerations (2). In an alternative approach the tip can be a reference electrode (e.g., a metal wire quasireference electrode or a drawn-out glass capillary connected to a true reference electrode via a salt bridge) and the potential at the tip monitored in the  $z$  direction or  $x$ - $y$  plane. This type of scanning potentiometry has already been employed at much lower resolution, for example, to probe corroding substrates (3-5). The use of an ultramicroelectrode (UME) to probe the diffusion layer concentrations by  $z$ -direction movement over a range of about 2-150  $\mu\text{m}$  by detecting substrate-generated species at the UME has been described recently (6).

We describe here several different types of experiments with the SECM. In principle SECM can provide surface topography information, potential distributions, and analytical data. Since electrochemical reactions occur in SECM, microfabrication can also be carried out with this apparatus. For example, etching and deposition of metals and semiconductors and synthesis (e.g., electropolymerization) are possible. Accounts of such applications have appeared (7, 8) and this area will not be discussed here.

## EXPERIMENTAL SECTION

**Apparatus.** A block diagram of the apparatus used for tip movement and control, which generally follows previous STM designs (1), is shown in Figure 2. In this apparatus the working electrode tip was held on a tripod ( $x'$ ,  $y'$ , and  $z'$ ) piezoelectric scanner. The substrate, held at a 45° angle to the tip axis, was carried by a movable  $x$ - $y$  stage which was moved independently by two piezoelectric translators (Burleigh Instruments, Fishers, NY, Type IW-502-2), which were controlled by a programmable controller (Type CE-2000-2A00). These permitted movements

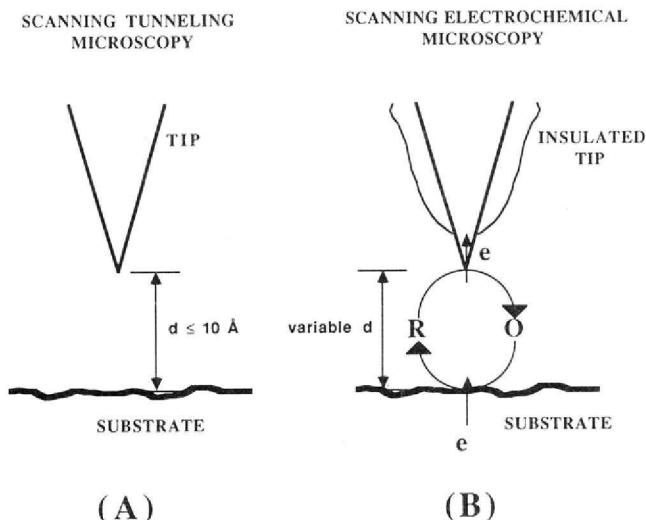


**Figure 1.** Comparison of scanning tunneling microscopy (STM) (A) and scanning electrochemical microscopy (SECM) (B).  $d$  is the spacing between tip and substrate.

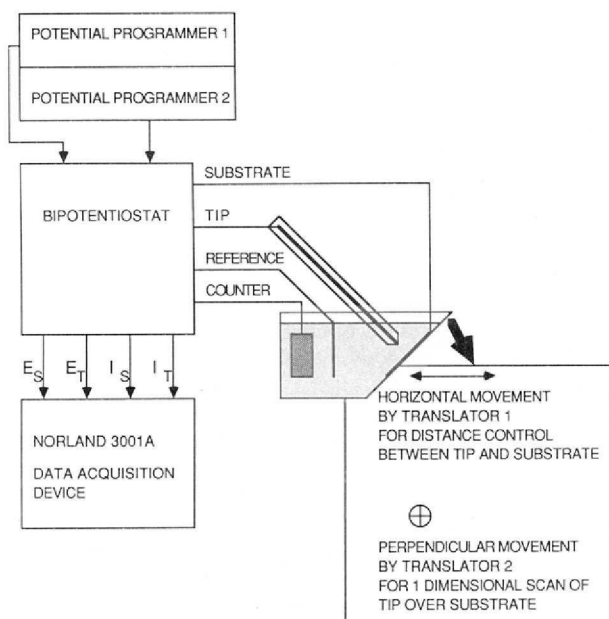


**Figure 2.** Block diagram of apparatus in dc experiment.

in the  $z$  direction of  $0.81 \mu\text{m}/\text{step}$  and in the  $x$  direction of  $1.22 \mu\text{m}/\text{step}$ . Higher resolution is obtained by acquisition of data during the step (from one step position to another). The tip potential ( $E_T$ ) and substrate potential ( $E_S$ ) were controlled vs a reference electrode, either a silver quasi-reference electrode (AgQRE) or a saturated calomel electrode (SCE) with a home-built bipotentiostat of conventional design (9) controlled with a Model 175 programmer (Princeton Applied Research, Princeton, NJ). The potentials,  $E_T$  and  $E_S$ , and the tip and substrate currents,  $i_T$  and  $i_S$ , were recorded with a four-channel data acquisition device (Digital Oscilloscope, Model 3001, Norland Corp., Fort Atkinson, WI). The data were either analyzed on the oscilloscope, employing the build-in functions, or transferred to a microcomputer (Apple Macintosh II or IBM XT) for analysis and plotting of the data.

The ac experiments were carried out with the apparatus shown in Figure 3. The phase angle between  $i_T$  and  $i_S$  and the relative magnitudes of the currents were obtained with a lock-in amplifier (Model 5206, Princeton Applied Research), which also supplied an ac potential, i.e., operating in the internal reference mode, to the substrate via the potentiostat. As shown in Figure 3, the tip potential was not controlled by the potentiostat but rather by a high-capacity SCE reference electrode in series with a battery power supply. This controlling circuit worked well as long as the tip current was very small (usually on the order of nanoamperes)

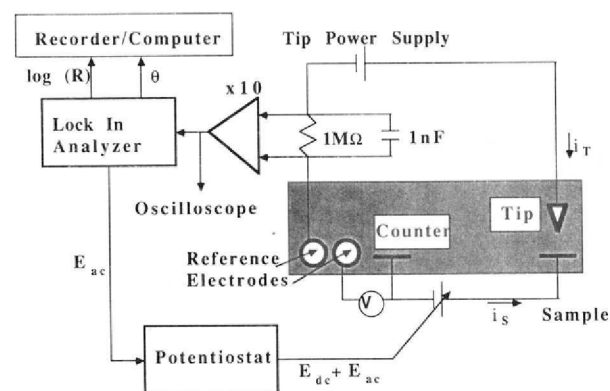


**Figure 3.** Block diagram of apparatus in ac experiments.

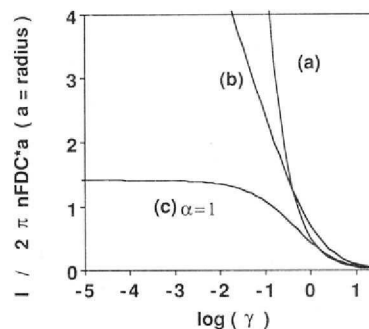


**Figure 4.** Representative steady-state current vs distance for generation/collection experiments for a planar substrate and different shaped tips: (a) planar disk; (b) spherical; (c) conical.

and the solution resistance was low.

**Tip Preparation.** Several different tips were used in these experiments. Construction of the Pt disk-in-glass ultramicroelectrodes (with 12.5- and  $5\text{-}\mu\text{m}$  radii) followed previous practice (10, 11) and is described in more detail elsewhere (12, 13).

Pt wire of the desired radius was washed with 30%  $\text{HNO}_3$  and dried overnight. This was placed in a 10 cm long, 1 mm i. d. Pyrex tube sealed at one end. The open end of the tube was connected to a vacuum line and heated with a helix heating coil for 1 h to desorb any impurities on the Pt. One end of the wire was then sealed in the glass by increasing the heating coil temperature. The sealed end was polished with sandpaper until the wire cross section was exposed, and then successively with 6-, 1-, and  $0.25\text{-}\mu\text{m}$  diamond paste (Buehler, Ltd., Lake Bluff, IL). Electrical connection to the unsealed end of the Pt wire was made with silver paint to a Cu wire. The glass-wall surrounding the Pt disk was conically sharpened by emery paper (Grit 600, Buehler, Ltd.) and  $6\text{-}\mu\text{m}$  diamond paste, with frequent checking by optical microscope until the diameter of the flat glass section surrounding the Pt disk was less than  $100 \mu\text{m}$ . This decreased the possibility of contact between glass and substrate because of any slight deviations in the axial alignment of the tip as the tip was moved close to the substrate. Carbon tips (10, 11) were used in the ac experiments. These were prepared from  $7 \mu\text{m}$  diameter C fibers that were burned slowly in a heating coil to decrease the diameter to 1–3  $\mu\text{m}$ . These were sealed in predrawn glass capillaries in a gas flame.

## RESULTS AND DISCUSSION

**Resolution and Tip Shape.** The ultimate resolution of the SECM depends primarily upon the tip size and shape. However, the solution resistance and mass and charge transfer process rates that affect the current density distribution are also important factors. Approximate expressions for the steady-state current that flows between substrate and tip as a function of  $z$  spacing for a conical and spherical tip in the generation/collection mode have been presented (14). The steady-state current mode would be of most interest for topographic information during  $x$ - $y$  scans. The approximate expressions for the steady-state current in the generation/collection mode, for example, in the configuration shown in

Figure 1B for different tip geometries above a much larger (assumed infinite) planar substrate are given below. Typical current ( $i$ )-distance curves are shown in Figure 4. For a planar tip, in the absence of edge effects, the familiar plane/plane thin layer expression, eq 1, applies (15)

$$i = nFADC^*/d \quad (1)$$

where  $d$  is the spacing between substrate and tip and  $C^*$  is the sum of the concentrations of oxidant,  $C_O$ , and of reductant,  $C_R$ .  $D$  is the diffusion coefficient (assuming  $D_O = D_R = D$ , in which  $D_O$  and  $D_R$  are the diffusion coefficients of oxidant (O) and reductant (R), respectively) and  $A$  is the electrode area. An actual planar disk electrode will show behavior more like a hemispherical electrode, especially when  $d \gg a$  (where  $a$  is the disk radius) (16, 17). Under these conditions, or when the tip actually has a spherical or hemispherical shape, the approximate expression for  $i$  is (14)

$$i = 2\pi nFDC^*r \ln [1 + (r/d)] \quad (2)$$

where  $r$  is the radius of the sphere. For a cone-shaped tip, the approximate current is given by (14)

$$i = 2\pi nFDC^*a^*(1 + \alpha^2)^{1/2}[1 - \gamma' \ln(1 + 1/\gamma')] \quad (3)$$

where  $\alpha = a^*/H$ , where  $a^*$  is the cone base radius and  $H$  is the height, and  $\gamma' = d/H$ . Note that in this latter case (Figure 4), the current becomes independent of tip-to-substrate spacing at very small  $d$  (as  $\gamma \rightarrow 0$ ) (14). Thus a conical or tapered cylindrical tip would be less useful than an inlaid disk or hemisphere for probing the topography of a substrate. Actual tips may have more complex shapes as are sometimes observed in ultramicroelectrodes (10, 11).

**Collection Experiments.** In the collection mode the tip is used as the detector only. The collection experiments can be performed in several operation modes. In the transient generation/constant potential collection (TG/CPC) mode, the potential of the substrate is stepped to a value,  $E_S$ , where an electrochemical reaction, for example, the oxidation  $R \rightarrow O + ne$ , occurs. The tip is held at a potential,  $E_T$ , where reduction of O back to R takes place. The tip current,  $i_T$ , is monitored as a function of time at constant  $z$ . The TG/CPC mode is analogous to transient experiments at the rotating ring-disk electrode (RRDE), where a product produced at the disk is swept convectively to the collector ring. With the TG/CPC mode it should be possible to calculate the distance between the tip and substrate from the time for the onset of the collection current, i.e., the time required for substrate-generated O to transit the gap and reach the tip. This approach has also been used to determine the concentration profile of oxidized species,  $C_O(z,t)$ , near a substrate for  $2 < z < 75 \mu\text{m}$  at  $0 < t < 4 \text{ s}$  by neglecting any distortion of the diffusion layer caused by the tip (6). A problem with this type of experiment is that the large current generated at the substrate by the potential step, which is composed of both non-faradaic (charging) and faradaic components, is coupled via the interelectrode capacitance and resistance to the tip and produces a transient tip current that interferes with the measurement of the faradaic  $i_T$ , especially at smaller  $t$  and  $z$ . This transient, in the direction of the substrate current, is clearly seen in the experiment in Figure 5 and makes it difficult to estimate the time for the onset of the collection current (i.e., the diffusional transit time between substrate and tip). The magnitude of this transient increased with the size of the substrate (i.e., with  $i_S$ ) and would be of greater importance as the transit time decreased, i.e., as  $z$  decreased.

Alternatively, the tip potential can be scanned while the substrate potential is changed. For example, a linear potential sweep can be applied to the tip to observe products generated at the substrate in the generation/cyclic voltammetric collection (G/CVC) mode. The observed tip current depends

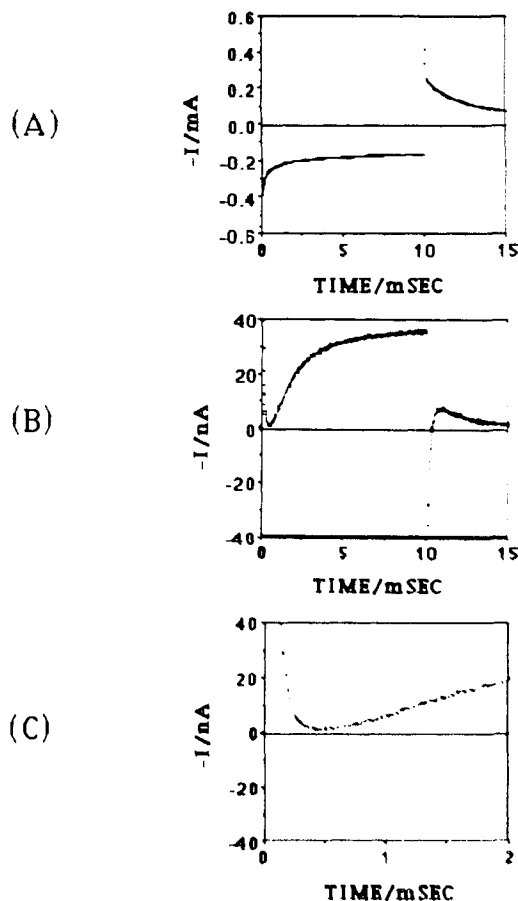


**Figure 5.** Substrate current ( $i_S$ ) (A) and tip current ( $i_T$ ) (B, C) for a 2.5 mm radius Pt disk substrate stepped from 0 to 1.0 V vs AgQRE with detection at a 5  $\mu\text{m}$  radius Pt disk tip held at 0 V vs AgQRE at a distance,  $d$ , of about 2.5  $\mu\text{m}$  from substrate. The solution was 2.5 mM ferrocene and 25 mM TBABF<sub>4</sub> in MeCN.

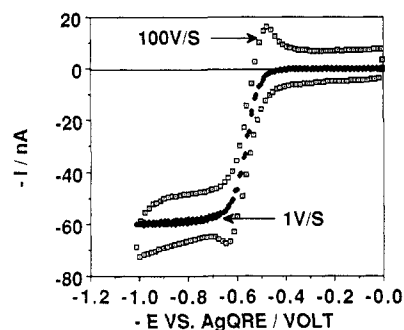


**Figure 6.** Cyclic voltammetry at 5  $\mu\text{m}$  radius Pt disk tip above a 2.5 mm radius Pt disk substrate held at  $E_S = 0.0 \text{ V}$  vs AgQRE with interelectrode separation,  $d$ , of 2.5  $\mu\text{m}$ . Solution contained 2.5 mM ferrocene and 25 mM TBABF<sub>4</sub> in MeCN.

upon the scan rate ( $v$ ),  $d$ , and  $E_S$ . Typical experimental curves for a 5  $\mu\text{m}$  radius Pt tip over a 2.5 mm radius Pt disk substrate in a solution of 2.5 mM ferrocene (Fc) in MeCN, 25 mM tetrabutylammonium fluoroborate (TBABF<sub>4</sub>) are shown in Figures 6 and 7. When  $d$  is large (e.g., 5 mm), the substrate has no effect upon the tip current, and typical ultramicroelectrode behavior (10, 11) is observed. At slow scan rates (e.g.,  $\leq 1 \text{ V/s}$ ), the anodic current for Fc oxidation attains a steady-state value given by (10, 11)

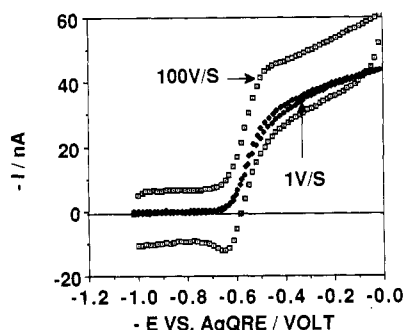
$$i = 4nFDC^*a \quad (4)$$

where  $a$  is the radius of the ultramicrodisk and  $C^*$  is the bulk concentration of Fc and no cathodic current appears. At fast scan rates (e.g.,  $\geq 100 \text{ V/s}$ ) a cyclic voltammogram closer to that expected of semiinfinite linear diffusion is obtained. When the tip is moved close to the substrate (e.g., ca. 2.5  $\mu\text{m}$ ),

**Table I. Phase Angle ( $\theta$ ) and Relative Amplitude ( $R$ ) Slopes for an ac Collection/Generation Experiment<sup>a</sup>**

frequency ( $f$ ), Hz	forward scan <sup>b</sup>				reverse scan <sup>c</sup>	
	$\partial\theta/\partial z$ , <sup>d</sup> deg $\mu\text{m}^{-1}$	$\partial \log R/\partial z$ , <sup>e</sup> $\mu\text{m}^{-1}$	$(\partial\theta/\partial z)/f^{1/2}$	$(\partial \log R/\partial z)/f^{1/2}$	$\partial\theta/\partial z$ , <sup>d</sup> deg $\mu\text{m}^{-1}$	$\partial \log R/\partial z$ , <sup>e</sup> $\mu\text{m}^{-1}$
0.75	3.0	0.0245	3.46	0.028	3.2	0.0245
1	3.64	0.029	3.64	0.029		
1.5	4.25	0.037	3.47	0.030	4.25	0.037
2	5.1	0.043	3.61	0.030	5.8	0.041
3	6.4	0.059	3.69	0.034	6.1	0.059
4	7.3	0.067	3.65	0.034	7.3	0.070
5	9.4	0.081	4.2	0.036	9.5	0.085

<sup>a</sup>Pt electrode substrate in 5 mM  $\text{K}_4\text{Fe}(\text{CN})_6$ , 5 mM  $\text{K}_3\text{Fe}(\text{CN})_6$ , 1 M KCl, modulated with 0.1 mA at frequency  $f$  with 6  $\mu\text{m}$  C tip at  $-0.3$  V vs SCE. <sup>b</sup>Tip moving toward substrate. <sup>c</sup>Tip moving away from substrate. <sup>d</sup>Slope of  $\theta$  vs  $z$  curve for  $z$  of 0 to 3.7  $\mu\text{m}$ . <sup>e</sup>Slope of  $\log R$  vs  $z$  curve.

**Figure 7.** As Figure 6, except  $E_s = 1.0$  V vs AgQRE.

as in Figures 6 and 7, the tip current depends upon the nature of the substrate and its potential. For example, when the substrate is held at 0 V (Figure 6),  $\text{Fc}^+$  generated at the tip is reduced to Fc and the anodic current is increased, compared to that when  $d$  is large. This feedback effect, discussed in more detail later, also results in a greater similarity of the anodic currents at large and small  $v$ . The cathodic current at larger  $v$  is reduced, since  $\text{Fc}^+$  generated at the tip is consumed at the substrate. When the substrate is held at 1.0 V and  $d$  is small (Figure 7), the anodic current is greatly decreased, since there is little unoxidized Fc in the region of the tip. The cathodic current is increased, since the tip is now acting in a collection mode, with the substrate acting as a generator of  $\text{Fc}^+$ . This CV mode of operation would be especially useful in identifying species or in elucidating the kinetics of unstable species dissolved from the substrate.

**ac Mode.** Another collection mode (called the ac generation/collection mode) involves applying an alternating potential or current variation to the substrate (optionally superimposed on a controlled dc substrate potential,  $E_s$ ) and determining the ac component of the tip current at a given  $E_T$  with a lock-in amplifier referenced to substrate signal. The principles of this technique and some preliminary experiments are included here. When an alternating current,  $i = I \sin \omega t$ , is applied to the conductive substrate electrode immersed in a solution containing both forms of a redox couple (O/R), the electrolysis that occurs induces a sinusoidal variation of the concentrations of O and R at the electrode surface. This type of electrolysis has been considered originally in connection with electrochemical studies by Warburg and Kruger and is treated, for example, by Vetter (18), where further details of the mathematical development can be found. The concentration variations in the vicinity of the substrate electrode surface are in the form of an exponentially damped sinusoid of the form ( $j = \text{O, R}$ ):

$$C_j(z,t) = C_j + A^* \exp(-z/z_0) \sin[\omega t - z/z_0 - \pi/4] \quad (5)$$

where  $z_0 = (2D/\omega)^{1/2}$ ,  $C_j$  is equilibrium concentration of  $j$  ( $j = \text{O, R}$ ), both with a diffusion coefficient,  $D$ ) and  $A^* = I/nF(D\omega)^{1/2}$ . The tip, held at a suitable potential, will sense the

local concentrations in the vicinity of the tip through variations in  $i_T$ . Thus from eq 5,  $i_T$  will vary with  $z$ , the tip distance from the substrate electrode, as an exponentially decaying sinusoidal function about a steady-state value. If  $i_T$  is measured with respect to the current applied to the substrate,  $i_s$ , e.g., with a lock-in amplifier, the following characteristics are expected: (1) The measured peak-to-peak tip current should decay exponentially with tip-to-sample distance,  $z$ . (2) The phase angle between the substrate and tip current,  $\theta = |z/z_0 + \pi/4|$ , should be proportional to  $z$  and should approach  $45^\circ$  as  $z \rightarrow 0$ . (3)  $\partial\theta/\partial z = (\omega/2D)^{1/2}$  and thus  $\partial\theta/\partial z$  varies as  $f^{1/2}$ , where  $f$  is the frequency of the applied ac ( $\omega = 2\pi f$ ). (4) The amplitude of the sinusoidal concentration wave,  $R = A^* \exp(-z/z_0)$ , so that  $|\partial \ln R/\partial z| = 1/z_0 = (\omega/2D)^{1/2}$ . Since the tip current is proportional to concentration,  $\partial \log i_T/\partial z$  should also vary as  $f^{1/2}$ .

Experiments were carried out to determine  $\partial \log R/\partial z$  and  $\partial\theta/\partial z$  as functions of  $f$ . These involved a 6  $\mu\text{m}$  diameter C tip above a Pt substrate immersed in a solution containing 5 mM each  $\text{K}_4\text{Fe}(\text{CN})_6$  and  $\text{K}_3\text{Fe}(\text{CN})_6$  in 1 M KCl. The applied ac peak substrate current was 0.1 mA (producing a variation of  $\pm 30$  mV around the rest potential) and  $E_T$  was  $-0.3$  V vs SCE. The modulation frequency,  $f$ , was set at a given value between 0.75 and 5 Hz, and  $\theta$  and  $R$  recorded from the lock-in amplifier outputs as the tip was advanced toward the substrate at a rate of 0.1  $\mu\text{m}/\text{s}$  and then retracted. Recordings of  $\theta$  vs  $z$  and  $\log R$  vs  $z$  were linear over the  $z$ -region investigated, 0–3.7  $\mu\text{m}$ . The slopes of these lines are listed in Table I. As predicted,  $\partial\theta/\partial z$  and  $\partial \log R/\partial z$  are proportional to  $f^{1/2}$ , with values of  $(\partial\theta/\partial z)f^{-1/2} = 3.59 (\pm 0.10)$  deg  $\mu\text{m}^{-1} \text{Hz}^{-1/2}$  and  $(\partial \log R/\partial z)f^{-1/2} = 0.031 (\pm 0.003)$   $\mu\text{m}^{-1} \text{Hz}^{-1/2}$  for  $f$  or 0.75–4 Hz. These values are close to those predicted from the relations for these values [i.e.,  $(1/\omega^{1/2}z_0)$  or  $(2D)^{-1/2}$ ], which in the same units are 3.64 deg  $\mu\text{m}^{-1} \text{Hz}^{-1/2}$  and 0.028  $\mu\text{m}^{-1} \text{Hz}^{-1/2}$ , respectively. At higher frequencies, the results deviated from these values, even though the values of  $\theta$  and  $R$  were reproducible for the tip advancing toward and retracting from the substrate, and  $\theta$  vs  $z$  and  $\log R$  vs  $z$  plots became nonlinear. Deviations were particularly pronounced in the longer distance region ( $\geq 3 \mu\text{m}$ ). These deviations can probably be attributed to some capacitive coupling between tip and substrate. Other factors that may be important in this mode of operation include feedback from the tip to substrate (not taken into account in eq 5) and the disturbance of the concentration profiles near the substrate surface caused by the tip. This latter effect will be especially important when the tip is scanned over the substrate. The nature of the tip, e.g., the quality of the seal between metal or carbon and the glass insulating sheath, is also an important factor in tip/substrate coupling, since poor sealing increases the tip capacitance.

These results suggest that the ac generation/collection mode, with measurements of  $\theta$  or  $R$ , can be used in scans of substrate surfaces. High resolution, based on the slopes of the  $\theta$  vs  $z$  and  $\log R$  vs  $z$  curves found here, will require application of higher modulation frequencies and smaller tips.

A preliminary experiment involving a scan with the 6- $\mu\text{m}$  C tip across a grid of 7- $\mu\text{m}$  Au wires spaced about 24  $\mu\text{m}$  apart showed small oscillations in  $\theta$  and  $\log R$  at the expected ca. 25  $\mu\text{m}$  spacing, but the resolution was poor. As suggested by a reviewer, application of ac approaches that decrease double layer capacitance contributions, e.g., second-harmonic methods, may be useful.

**Feedback Experiments.** In the feedback mode a potential is applied to the moving tip which is used as both the source and the detector; the tip current ( $i_T$ ) is a function of the nature of the substrate and the distance between substrate and tip. When the substrate is conductive or semiconductive, the oxidized form, O, formed at the tip can be reduced at the substrate producing R, which diffuses back to the tip. This causes  $i_T$  to be higher than it is when the tip is far ( $d \rightarrow \infty$ ) from the substrate. The magnitude of this "feedback" component of the current is a function of the distance between the generator tip and the substrate (the smaller  $d$ , the larger the feedback current). This type of feedback effect is unique to closely spaced electrodes in quiescent solutions, e.g., it is not found with the RRDE where hydrodynamic flow from disk to ring prevents any detectable disk feedback current and has been addressed experimentally and theoretically at microelectrode arrays (18, 19). One can think of this as a form of "electrochemical radar", where the wave of O generated at the tip interacts at the substrate to "reflect back" a wave of R that is detected at the tip. As opposed to actual radar, which is basically a transient technique, this feedback mode can also be used at steady state. This mode has the advantage over the transient collection mode in that the coupling transient is absent, since only measurements at the tip are made, permitting the examination of very small distances and short times. Moreover, the feedback mode is also useful when the substrate cannot be conveniently held at an externally applied potential (e.g., when it is a small isolated conductive zone) or when application of a potential might cause undesirable reactions or decomposition of the substrate (e.g., for Pt sputtered on mica (21), where hydrogen evolution can cause the Pt to peel off). In the feedback mode the substrate itself need not necessarily be connected to an external potential source (e.g., a potentiostat), because most of the conductive substrate is located away from the tip reaction and is bathed in a solution containing mainly R, maintaining it at a potential negative to the formal potential,  $E^\circ$ , of the O/R couple. In this case, the localized reduction current at the portion of the substrate under the tip can be driven by the oxidation of R at those portions of substrate away from the tip region. The feedback mode can also be applied to an insulating substrate, as discussed in the next section.

We will describe several experiments in the feedback mode and give a more quantitative treatment of the feedback current at the tip. Consider the current at an ultramicroelectrode ( $a = 5 \mu\text{m}$ ) immersed in a solution of 2.5 mM Fc in 25 mM TBABF<sub>4</sub>, MeCN over a 2.5-mm Pt disk substrate (Figure 8). When the tip is far ( $>100 \mu\text{m}$ ) from the substrate,  $i_T$  is not affected by the presence of substrate;  $i_T(d \rightarrow \infty)$  is given by eq 4 (10, 11). When the tip is close to the substrate, i.e., as  $d \rightarrow 0$ , the tip current can be approximated by eq 1 or with  $A = \pi a^2$  by

$$i_T(d) = nFDC \cdot \pi a^2 / d \quad (6)$$

Normalizing  $i_T(d)$  with respect to  $i_T(d \rightarrow \infty)$  yields

$$i_T(d)/i_T(d \rightarrow \infty) = (\pi/4)(a/d) \quad (d \rightarrow 0) \quad (7a)$$

$$i_T(d)/i_T(d \rightarrow \infty) = 1 \quad (d \rightarrow \infty) \quad (7b)$$

As shown in Figure 8, the theoretical computer simulation curve (22) fits the experimental results quite well. The curve exhibits an expected straight line (eq 7a) at small  $d$  and  $i_T$ -

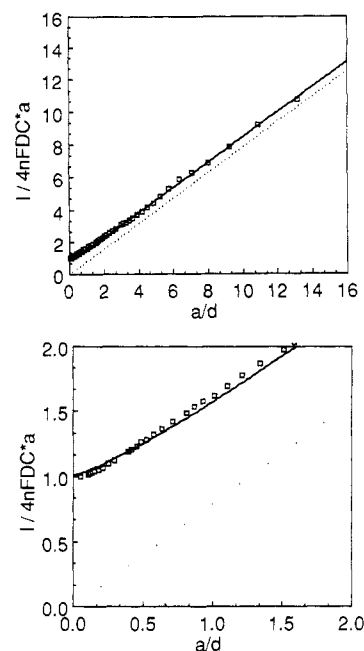


**Figure 8.** Normalized current vs  $a/d$ , where  $a$  = tip radius (5  $\mu\text{m}$ ). Dotted line with zero intercept is plot of thin layer eq 1. Solid curve is the computer-simulated theoretical curve. Experimental data are shown by open squares.

( $d$ )/ $4nFDC \cdot a$  deviates to 1 (eq 7b) at large  $d$ . With this calibration curve the distance between substrate and tip can be found from the measured tip current and known tip diameter. Thus,  $i_T$ , which varies as  $1/d$ , is a measure of distance,  $d$ , as compared to the situation in STM, where the tunneling current varies as  $\exp(-\text{const } d)$  (1).

The feedback mode can also be used with a nonconductive substrate. In this case,  $i_T$  is perturbed because the substrate interferes with the essentially hemispherical diffusion field to the tip, causing a decrease in  $i_T$  as the tip-to-substrate distance is decreased. When the tip gets close to the insulating substrate, diffusion to the tip is hindered (i.e., a portion of the hemispherical diffusion zone is blocked). To demonstrate this effect, preliminary experiments were carried out with a 50  $\mu\text{m}$  diameter glass fiber on glass microscope cover slip substrate (Figure 9). When the tip was above (ca. 60  $\mu\text{m}$ ) the cover slip, the current was slightly smaller than  $i_T(d \rightarrow \infty)$  (17.3 nA). As the tip was scanned over the 50- $\mu\text{m}$  fiber, the current decreased because the fiber interfered with diffusion to the tip. This decrease in current was smaller when the tip was scanned at a larger distance above the fiber (Figure 9B). Note that the width (in time) of the current decrease region corresponds approximately to that of the fiber at this scan rate ( $dx/dt$ ) and that the symmetrical shape of the  $i_T$  vs  $t$  (or  $x$ ) is that expected for the circular cross section of the glass fiber. Moreover, the  $i_T$  vs  $t$  trace, when the tip scan direction is reversed, is essentially the mirror image of the forward scan at both values of  $d$ . The ability to examine an insulating substrate is unique to this mode of operation and to the SECM as compared to the STM. Insulators can be examined by the atomic forces microscope based on different principles (23).

Thus the in feedback mode, the difference in the conductive nature of the substrate determines whether  $i_T > i_T(d \rightarrow \infty)$  (conductor) or  $i_T < i_T(d \rightarrow \infty)$  (insulator). To demonstrate this effect on a substrate with both types of regions, the tip was scanned above a structure made by folding a 40  $\mu\text{m}$  thick Pt foil, insulating between the folds with epoxy cement, and cementing this between two glass microscope slides (Figure 10B). The surface of this structure was polished flat with sandpaper (grit 600) and 5- $\mu\text{m}$  diamond paste. When the tip

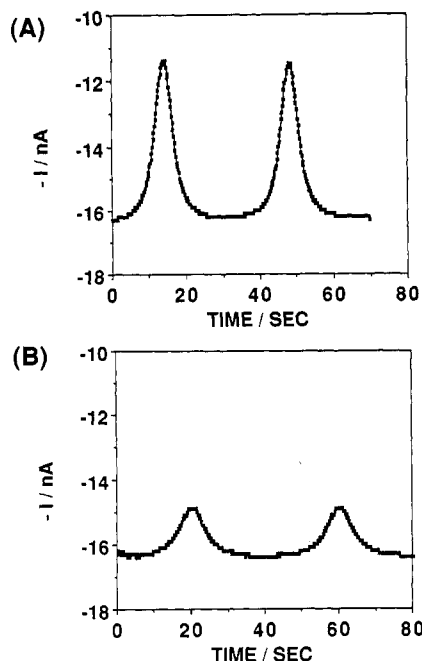


**Figure 9.** (A) Tip current for 5  $\mu\text{m}$  radius Pt disk held at  $d < 60 \mu\text{m}$  from a glass substrate with a 50  $\mu\text{m}$  diameter glass fiber and scanned at 6  $\mu\text{m/s}$ .  $E_T = 1.0 \text{ V}$  vs AgQRE. Solution as in Figure 6. Scan direction reversed at 30 s. (B)  $d > 68 \mu\text{m}$ , scan direction reversed at 40 s.

was scanned ( $d < 10 \mu\text{m}$ ) above the glass region,  $I_T$  was smaller than the  $i_T(d \rightarrow \infty)$  of 17.3 nA (Figure 10A). When the tip was above the conductive Pt region,  $i_T > i_T(d \rightarrow \infty)$ , with the epoxy region represented by a current dip. Again, the pattern produced a mirror image when the scan direction was reversed.

This SECM feedback approach is potentially a powerful one for obtaining a two-dimensional ( $x$ - $y$ ) scan across a surface with both conductive and insulating regions. Scans with the substrate held at different potentials may also be informative in distinguishing different conductive regions with different heterogeneous electron transfer rates for the substrate reaction ( $\text{O} \rightarrow \text{R}$ ). Under these conditions the choice of the redox couple ( $\text{O}/\text{R}$ ) will be important. The couple should also be selected with regard to the chemical nature of the substrate, i.e., couples with very positive  $E^\circ$  values should be avoided with oxidizable substrates, such as copper and couples that might cause gas evolution, e.g.,  $\text{MV}^{2+}/+$  ( $\text{MV}^{2+}$  = methyl viologen), should not be used with Pt substrates, where  $\text{H}_2$  formation could occur. This would be especially important with substrates such as Pt on mica, which are unstable in the hydrogen evolution region. Although the resolution seen here is low, because the tip diameter is rather large, the principles demonstrated should apply with smaller tips. As with the STM, the tip shape is important in obtaining good resolution.

### CONCLUSIONS

The results given here suggest that SECM can be employed to investigate surfaces immersed in liquids with good resolution. Although the  $x$ - $y$  resolution demonstrated here is only of the order of micrometers, improvements in tip preparation and control should allow higher resolution to be obtained. The preparation of flat, small, disk-shaped electrodes surrounded by a thin insulating layer is probably the most important factor in improving the resolution. Another problem that must be considered as the tip is scanned above a substrate is the perturbation of the diffusion layer by the tip structure itself. Clearly, the smaller the tip, the less the diffusion layer perturbation will be. The feedback mode seems to be especially useful for several reasons. It can be applied with both conductive and nonconductive substrates and will probably be

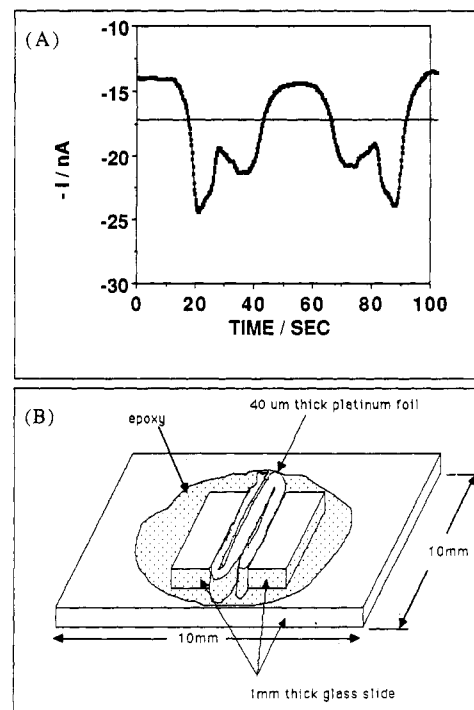


**Figure 10.** (A) Tip current for 5  $\mu\text{m}$  radius Pt disk scanned at 6  $\mu\text{m/s}$  about 10  $\mu\text{m}$  above a Pt/glass structure shown in (B). Conditions as in Figure 6. Scan direction reversed at 60 s.

less sensitive to the tip perturbation effects mentioned above, since the diffusion layer of interest in the measurement originates at the tip rather than at the substrate. It should also be less sensitive to interelectrode and external coupling effects and to charging current perturbation.

Although the results discussed here emphasized only electrochemical measurements in SECM, other modes of operation should be possible. For example, electrogenerated chemiluminescence (ECL) (24) or inverse photoemission spectroscopic (IPS) (25, 26) modes of investigating conductive substrates would involve detection of light emitted as the tip is scanned across the surface with tip and substrate potentials adjusted to generate suitable intermediates. Similarly, an electroluminescent (EL) method might be of interest in the investigations of semiconductors (27, 28). Note that in these methods the resolution attainable is a function of the tip size and distance from substrate rather than the wavelength of the emitted radiation. Alternatively, the effect of irradiating the substrate (e.g., a semiconductor) with suitable radiation (larger than the band gap) and recording the tip photocurrent as a function of tip position might be useful in the mapping of a surface in photoelectrochemical (PEC) experiment. This would be analogous to the technique previously described where a laser beam was rastered over a semiconductor surface to obtain information about surface states and structures (29). Note that this PEC mode of operation has already been employed to etch thin lines in a GaAs substrate immersed in solution (8).

### LITERATURE CITED

- (1) Binnig, G.; Rohrer, H. *Helv. Phys. Acta* **1982**, *55*, 726-735.
- (2) Bard, A. J.; Faulkner, L. R. *Electrochemical Methods, Fundamentals and Applications*; Wiley: New York, 1980; Chapter 1.
- (3) Isaacs, H. S.; Kendig, M. W. *Corrosion* **1980**, *36*, 269-274.
- (4) Isaacs, H. S.; Vyas, B. In *Electrochemical Corrosion Testing*, ASTM STP 727; Mansfeld, F.; Bertocci, U., Eds.; American Society for Testing and Materials: Philadelphia, PA, 1981; pp 3-33.
- (5) Rosenfeld, I. L.; Danilov, I. S. *Corros. Sci.* **1987**, *7*, 129-142.
- (6) Engstrom, R. C.; Meany, T.; Tople, R.; Wightman, R. M. *Anal. Chem.* **1987**, *59*, 2005-2010.
- (7) Lin, C. W.; Fan, F.-R. F.; Bard, A. J. *J. Electrochem. Soc.* **1987**, *134*, 1038-1039.
- (8) Craston, D. H.; Lin, S. W.; Bard, A. J. *J. Electrochem. Soc.* **1988**, *135*, 785-786.



- (9) Bard, A. J.; Faulkner, L. R. *Electrochemical Methods, Fundamentals and Applications*; Wiley: New York, 1980; p 567.
- (10) Wightman, R. M.; Wipf, D. O. In *Electroanalytical Chemistry*; Bard, A. J., Ed.; Marcel Dekker: New York, 1988; Vol. 15.
- (11) Fleischmann, M.; Pons, S.; Rollson, D.; Schmidt, P. P. *Ultramicroelectrodes*; Datatech Systems: Morgantown, NC, 1987.
- (12) Garcia, E.; Kwak, J.; Bard, A. J. *Inorg. Chem.*, in press.
- (13) Kwak, J. Ph.D. Dissertation, The University of Texas at Austin, 1989.
- (14) Davis, J. M.; Fan, F.-R. F.; Bard, A. J. *J. Electroanal. Chem.* **1987**, *238*, 9-31.
- (15) Hubbard, A. T.; Anson, F. C. In *Electroanalytical Chemistry*; Bard, A. J., Ed.; Marcel Dekker: New York, 1970; Vol. 4, p 129.
- (16) Albery, W. J.; Hitchman, M. L. *Ring-Disc Electrodes*; Clarendon Press: Oxford, 1971.
- (17) Bruckenstein, S.; Miller, B. *Acc. Chem. Res.* **1977**, *10*, 54-61.
- (18) Vetter, K. J. *Electrochemical Kinetics*; Academic Press: New York, 1967; pp. 200-213.
- (19) Bard, A. J.; Crayston, J. A.; Kittlesen, G. P.; Varco Shea, T.; Wrighton, M. S. *Anal. Chem.* **1986**, *58*, 2321-2331.
- (20) Varco Shea, T.; Bard, A. J. *Anal. Chem.* **1987**, *59*, 2101-2111.
- (21) Liu, H.-Y.; Fan, F.-R. F.; Bard, A. J. *J. Electrochem. Soc.* **1985**, *132*, 2666-2668.
- (22) Kwak, J.; Bard, A. J. manuscript in preparation.
- (23) Binnig, G.; Quate, C. F.; Gerber, C. *Phys. Rev. Lett.* **1986**, *56*, 930-933.
- (24) Bard, A. J.; Faulkner, L. R. In *Electroanalytical Chemistry*; Bard, A. J., Ed.; Marcel Dekker: New York, 1977; Vol. 10, Chapter 1.
- (25) MacIntyre, R.; Sass, J. K. *J. Electroanal. Chem.* **1985**, *196*, 199-202.
- (26) Ouyang, J.; Bard, A. J. *J. Phys. Chem.* **1987**, *91*, 4058-4062.
- (27) Beckmann, K. H.; Memming, R. *J. Electrochem. Soc.* **1969**, *116*, 368-373.
- (28) Fan, F.-R. F.; Leempoel, P.; Bard, A. J. *J. Electrochem. Soc.* **1983**, *130*, 1866-1875.
- (29) Folmer, J. C. W.; Turner, J. A.; Parkinson, B. A. *Inorg. Chem.* **1985**, *24*, 4028-4030.

RECEIVED for review September 12, 1988. Accepted October 17, 1988. The support of this research by the Robert A. Welch Foundation and the Texas Advanced Technology Research Program is gratefully acknowledged. We thank the U.S.-Israel Education Foundation for providing a Fulbright Fellowship to O. Lev.

## Raw Materials Testing Using Soft Independent Modeling of Class Analogy Analysis of Near-Infrared Reflectance Spectra

Paul J. Gemperline\* and Laurie D. Webber

Department of Chemistry, East Carolina University, Greenville, North Carolina 27858

Frank O. Cox

Analytical Development Laboratories, Burroughs Wellcome Co., Greenville, North Carolina 27835-1887

**A method for testing raw materials has been developed by using SIMCA (soft independent modeling of class analogy) analysis of near-infrared reflectance spectra. Samples are classified as acceptable or unacceptable based on probability levels obtained from an *F* test. Over 400 first derivative spectra of six types of pharmaceutical raw materials were tested. The method had an overall recognition rate of 95 % for acceptable samples and a 99 % rejection rate for unacceptable samples. The single unacceptable sample classified incorrectly differed from the "training" samples only in particle size distribution. Minor levels (ca. 1 %) of contaminants were detected. Materials rejected during the manufacturing process by manual testing were detected. Subclustering with respect to suppliers was investigated. Sources of variation in the spectra were analyzed, including short-term and long-term instrumental variation, variation due to cell repacking, and variation between production lots.**

### INTRODUCTION

Near-infrared reflectance (NIR) spectroscopy has become recognized as a rapid and sensitive method of analysis of organic materials. The near-infrared spectral region, which spans from 1100 to 2500 nm, has high information content in the form of numerous overlapped absorption bands arising from overtones and combinations of X-H stretching modes of vibration (*1*). Research conducted by Norris and co-workers in the 1960s indicated that NIR spectroscopy was applicable to the quantitative analysis of moisture, protein, starch, lipid, and fiber content in grain and forage crops (*2, 3*). Near-infrared reflectance analysis (NIRA) has now found numerous applications in the food-processing, textile, cosmetic, clinical,

polymer, agricultural products, and pharmaceutical industries (*3-7*).

This widespread use of NIR spectroscopy can be greatly attributed to the introduction of powerful computerized data processing techniques for quantitative interpretation of the complicated NIR spectra. Multiple linear regression has been the most frequently used technique for quantitation (*2, 3, 5, 8*); however, partial least squares and principal component regression have also been reported as successful computational methods for interpretation of the spectra (*9-11*).

Unfortunately, these techniques do not lend themselves well to qualitative determinations. Lodder, Hieftje, and Selby have recently reported advances in detection of capsule and tablet tampering (*12, 13*). The pattern recognition technique called BEAST, the acronym for bootstrap error-adjusted single-sample technique, was used for analysis of NIR spectra of capsules and tablets. The capsule and tablet adulterants detected in their research included KCN, NaCN, NaF, As<sub>2</sub>O<sub>3</sub>, Fe<sub>2</sub>O<sub>3</sub>, and aluminum shavings. Linear discriminant analysis and Mahalanobis distance techniques have also been used for qualitative identification of materials (*14*). Both methods require selection of an optimal set of discriminating wavelengths, either by visual means when only a few compounds are being analyzed or by computer analysis when the number of training set classes becomes larger. In linear discriminant analysis (LDA), the spectra of samples are classified by finding a linear function that separates categories of spectra based on their absorbances at optimal wavelengths. When optimal pairs of wavelengths are used as *X, Y* plotting coordinates, samples tend to cluster by category. Ideally, easily separated clusters are observed for each category of material. The major shortcoming of this technique is the inability to recognize samples that are outliers. Mark and Tunnell report the superiority of a method using Mahalanobis distances for